Hindawi
Advances in Civil Engineering
Volume 2021, Article ID 8894713, 12 pages
https://doi.org/10.1155/2021/8894713

Research Article

Characteristics of Karst Cave Development in Urban Karst Area and Its Effect on the Stability of Subway Tunnel Construction

Fei Xue, Minjun Cai, Tianzuo Wang, and Tongyang Zhao

College of Civil Engineering, Key Laboratory of Rock Mechanics and Geohazards of Zhejiang Province, Shaoxing University, Shaoxing 312000, China

Correspondence should be addressed to Tianzuo Wang; wangtianzuo@usx.edu.cn

Received 28 September 2020; Revised 15 April 2021; Accepted 28 April 2021; Published 8 May 2021

Academic Editor: Liborio Cavaleri

The existence of karst caves poses a large threat to safe tunnel construction in a karst area. This paper presents a synthetic method to evaluate the collapse risk before subway tunnel construction with Yang-Jian interval tunnel as a case study. The crosshole seismic Computed Tomography (CT) integrated with Geological Drilling (Geo-D) was first applied to accurately delineate the karst location and its scale. Then, 483 groups of seismic wave CT images were recorded, and 524 karst cave anomalies were found. The height of karst caves in the study area is 1–20 m and mainly concentrated at approximately 5 m. The vertical distance between the karst cave and the tunnel is mainly within 15 m. According to the detection results, a series of numerical models were built and calculated using FLAC3D to investigate the effect of different sizes and locations of karst caves on the displacement and stability of the surrounding rock in tunnels. Afterwards, based on the simulation results, the disturbance degree evaluation index was established to quantitatively evaluate the risk level of karst caves. The evaluation results indicate that the buried depth of the karst cave greatly affects the disturbance degree. No treatment is required for the deeply buried karst cave that is more than 7 m from the tunnel. When the distance between the cave and the tunnel is less than 7 m, there is a critical size of the cave. Karst caves that are larger than that critical value must be filled with a single slurry or binary slurry before tunnel construction to eliminate the risk of tunnel collapse. This study can be used to provide a more efficient and economical program for metro tunnel construction above a karst cave.

1. Introduction

Karst collapse is a type of karst dynamic geological action and phenomenon, where the rock and soil above the karst caves are deformed and destroyed under the action of natural or human factors, and collapse pits (holes) are formed on the ground. Karst areas are widely distributed in China and account for approximately 1/3 of the country's area. The existence of karst caves causes severe threats and challenges to the safe construction of subway tunnels and other underground space projects due to the probability of collapse, water and mud inrush, and other serious geological hazards that may occur during the construction [1–3]. It is well known that underground karst structures generally have complex distribution characteristics with different sizes, locations, and filling degrees, which significantly affect the stability of the surrounding rock. In fact, the risk of tunnel collapse increases with the increase in the size of the karst and the decrease in the distance between karst and tunnel [3]. Thus, not all karst caves pose a larger threat to the construction safety of the tunnel, and the safety of the project can be guaranteed by only taking the relevant treatment measures for the more dangerous karst caves instead of all karst caves. The crux of building a metro tunnel in karst areas lies in accurately detecting the karst distribution characteristics and estimating the stability of the surrounding rock in tunnels as affected by karst caves.

With regard to the detection technology of karst caves, a great deal of researches have been done to accurately predict the hazardous geological conditions during tunnel construction in karst terrains. Nowadays, the commonly used detection technologies mainly include two categories: destructive methods such as the Core Drilling and Percussion Drilling [4] and nondestructive methods including the

Ground Penetrating Radar (GPR) [5–7], Electrical Resistance Topography (ERT) [8, 9], Tunnel Seismic Prediction (TSP) [10–12], crosshole seismic Computed Tomography (CT) [13, 14], and Transient Electromagnetic Method (TEM) [8, 9, 15]. For example, Gómez-Ortiz and Martín-Crespo had applied shallow and noninvasive geophysical techniques, that is, GPR and ERT, to ascertain the existence and characteristics of cavities and galleries. It shows that GPR and ERT techniques are useful to detect underground cavities [16]. Carrière et al. had also applied GPR and ERT to interpret water transfer and storage within the karst unsaturated zone [17]. Cardarelli et al. combined ERT and SRT and used these to determine the location of cavities [18]. Generally, GPR, ERT, and TEM are belonging to near-surface geophysical exploration measures which are more suitable for detecting shallow targets, and their resolutions are highly dependent on the depth of the cavity and thickness of the layered material [19]. In karst terrains where the conductivity of the underground overburden is poor, crosshole seismic CT is the most frequently used method because it can provide a detailed view of the subsurface, which is particularly important at depths that near-surface detection techniques cannot sufficiently permeate [20].

In terms of the stability of surrounding rock in tunnels as affected by karst caves, the investigation on this topic has attracted the attention of many researchers. Li et al. reported a possible method to predict the top of a concealed karst cave based on displacement monitoring during tunnel construction. The numerical calculation was also carried out to discuss the surrounding rock deformation affected by the top karst cave during tunnel excavation, and it was found that the simulation results were consistent with those predicted by the proposed method [3]. Zhao et al. studied the stability of a rock pillar on a concealed karst cave ahead of a roadway. Based on a fluid-solid coupling method and strength reduction method, a fluid-solid coupling model was developed to calculate the safety thickness of a rock pillar for preventing water inrush from a concealed karst cave [21]. Cui et al. presented a procedure for karst cave treatment to mitigate potential geohazards during shield tunneling in karst regions. The karst cave treatment procedure was successfully applied to the Guangzhou metro tunnel [22]. By simplifying the top karst cave to a beam-slab model, Song established a numerical solution of the minimum safe thickness of the tunnel roof and floor by adopting elastic theory [23]. Based on the strength reduction method, energy catastrophe theory, and dichotomy, Lai investigated the safe distance between the concealed karst cave and the tunnel. A comparison of these three methods showed that the numerical solution of catastrophe theory was the most reasonable [24]. In order to predict the collapse of rock mass where a tunnel is excavated above a karst cave, Fu et al. derived an analytical expression of the collapse surface from variational calculation in the framework of the upper bound theorem. This analytical solution was then applied for investigating the effects of rock parameters on the collapse surface of the rock mass where a karst cave exists beneath a tunnel. The analytical solution matched up with numerical solution very well, so as to provide an effective method for collapse risk prediction of karst tunnels [25].

However, all of the above studies only focus on single respect. A comprehensive investigation, which detects the karst distribution characteristics and estimates the stability of the surrounding rock in the tunnel excavation process, is rarely reported. This paper is concerned with providing comprehensive guidance for construction where there is a karst cave beneath a metro tunnel. The crosshole seismic CT integrated with Geological Drilling (Geo-D) was first applied to accurately delineate the karst location and its scale. According to the detection results, the numerical calculation was performed to investigate the effect of different sizes and locations of karst caves on the displacement and stability of surrounding rock in tunnels using FLAC3D. The simulation results were used to evaluate the risk levels of karst caves with different sizes and locations. This study can be used to provide a more efficient and economical program for metro tunnel construction above a karst cave.

2. Background of the Studied Area

The 964 m-long Yang-Jian subway tunnel, which is located between the sections of 43.789 km and 44.754 km (K43 + 789–K44 + 754), is one of the interval tunnels of the fourth section of urban rail transit line 1 in Shaoxing city, Zhejiang province, China (see Figure 1). This tunnel is constructed by the shield method with an external diameter of 6.7 m and an overburden thickness of 11.3–13.3 m. This section is located in the lacustrine-alluvial plain area of the north Zhejiang Plain with slightly flat terrain. The existing floor elevation is approximately 5.50–6.93 m. The studied area terrain gradually rises from north to south, and the underlying bedrock is buried deeper and shallower from north to south. Thus, the studied area topography is favorable for the accumulation and concentration of groundwater.

According to the preliminary geological investigation, the karst topography in the Yang-Jian interval tunnel is especially well developed both horizontally and vertically. The thickness of the Quaternary overburden in this site is approximately 17.7–25.4 m, and the underlying basement lithology is dominated by limestone of the middle Cambrian Yang Liugang Formation (∈2y), which belongs to the category of solvable rocks. Due to the effect of structures and folds, there are many pores and fissures in the rock. Moreover, the site has rich dissolution capacity and controllable groundwater. The measured level of karst water at the site is 2.6 m deep, and it is under pressure. The fault structure is developed, and the tectonic movement is dominated by oscillatory lifting movement.

3. Characteristics of Karst Development in This Area

3.1. Geophysical Detection Methods. Due to the relatively thick karst overburden and strong environmental interference such as electromagnetic, stray current, and vibration

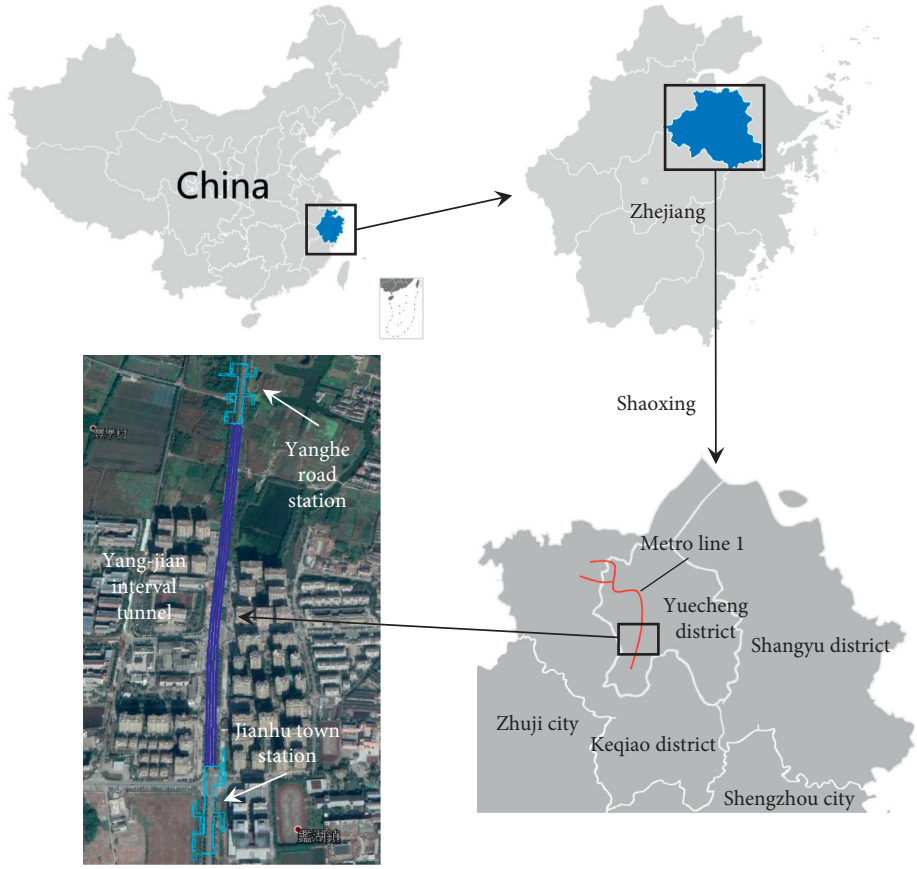

Figure 1: Location of the studied area.

interference, in this field areas, to identify a more accurate view of karst location and its scale, the crosshole seismic CT method integrated with Geo-D was used, and the survey layout is presented in Figure 2. As shown in Figure 2, three rows of detection geological boreholes, 189 boreholes with a drilling depth of 40–65 m, and a borehole spacing of approximately 15 m were arranged in the direction of the subway line to perform combined observation between one borehole and ambient boreholes, which effectively reduced the number of boreholes and drilling costs. As illustrated in Figure 3, all seismic CT profiles were recorded along survey lines (the pink line in Figure 2) using the Geode96 seismograph (manufactured by Geometrics Inc.) with a sample rate of 0.02 ms. The TD-Sparker50 KJ electric spark transmitter (produced by Beijing Tongdu Technology Co., Ltd.) was applied as the seismic source with an excitation source frequency of 20–300 Hz, a maximum emitting energy of 5 KV, and a trigger interval of 1 m.

Data processing consisted of the following steps: First, the shortest-path ray-tracing method and least square conjugate gradient method (SIRT) were used to interpret the seismic data. Second, the wave velocity of each stratum unit, contour map, and chromatic scale map of the entire section of the stratum velocity were obtained based on the seismic CT inversion fitting calculation results. Third, according to the wave velocity contour map, the low-speed geological anomalies were delineated, and the development scope and scale of karst were deduced by combining the geological and borehole data.

3.2. Karst Detection Results. According to the ultrasonic test results of the borehole data and limestone samples, the velocity range of the formation interpretation by the elastic wave CT can be determined as follows: the wave velocity of overburden is 1400–2600 m/s, the wave velocity of fully ~ strongly and moderately weathered bedrock is 2600–3500 m/s, and the wave velocity of moderately weathered bedrock is greater than 3500–5000 m/s, and the wave velocity of the karst cave is 2000–3200 m/s, where the wave velocity of the unfilled or underfilled karst cave is 2000–2800 m/s and that of the dense filling karst caves is 2,800–3,200 m/s.

The typical inversion wave velocity chromatograms are presented in Figure 4. Different wave velocities are displayed in different colors. As shown in Figure 4(a), the boundary between the upper overburden low-speed zone and the underlying bedrock high-speed zone is relatively clear, and there is no low-speed abnormal zone in the moderately weathered bedrock. Thus, there is no karst cave development in the XZ29-XD32 profile. However, when karst caves develop between detected profiles, the overall seismic waves

Figure 2: Layout sketch of the prospecting boreholes and survey lines.

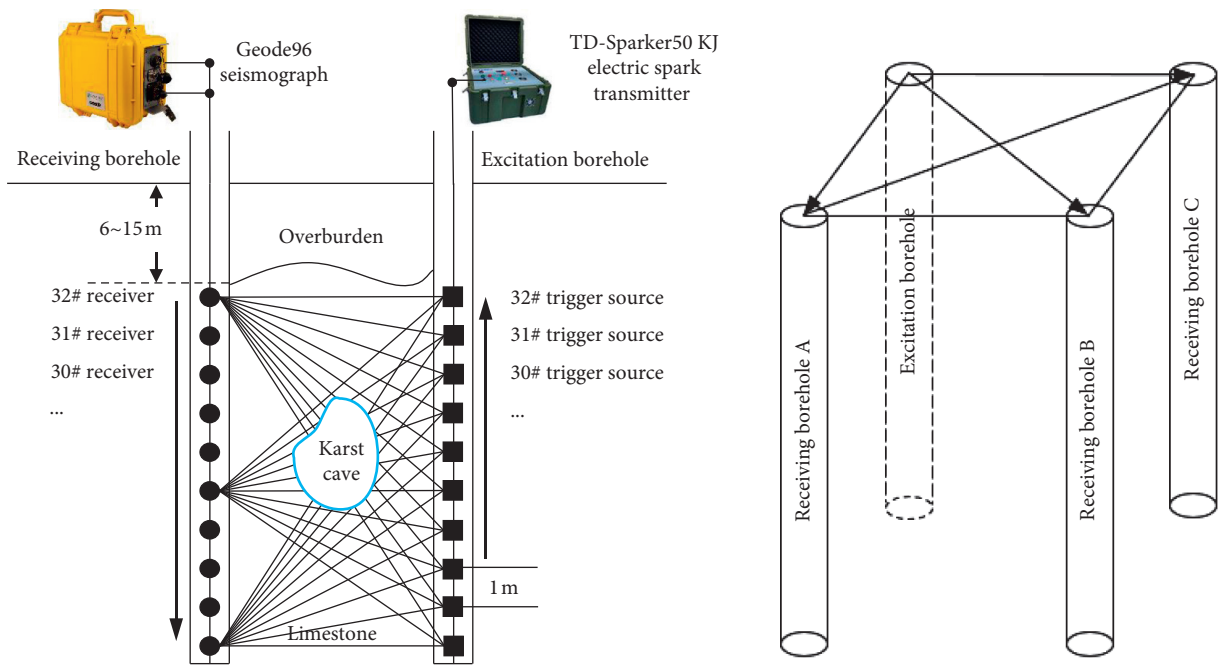

Figure 3: Schematic diagram of the detection system configuration and work principles of crosshole seismic CT.

show a decrease in velocity. In Figures 4(b) and 4(c), there are several low-velocity abnormal areas in the moderately weathered bedrock. From the elastic wave CT velocity profile of the central borehole and surrounding boreholes, the development and distribution area (the blue lines) of the cavern were further spatially defined.

Based on these interpretation principles, 483 groups of seismic wave CT inversion images were interpreted, and 524 karst cave anomalies were found. The typical cross-section view of karst geology revealed is provided in Figure 5. To more clearly explain the distribution characteristics of karst geology in this area, 524 detected karst abnormal bodies were counted according to the size and location of the karst caves, and the statistical results are shown in Figure 6. In Figure 6(a), most karst caves in the study area are within 5 m high, which account for more than 85% of the total number. Karst caves with heights of 6–10 m account for 13% of the total, and those with heights greater than 10 m only account for approximately 1% of the total. In most revealed karst caves (Figure 6(b)), the vertical distance between the karst cave and tunnel is mainly within 15 m, among which 6–10 m accounts for the largest portion (33.6%).

4. Effect of the Karst Cave Size and Location on the Stability of Tunnel

4.1. Numerical Model. To investigate the effect of karst caves with different sizes and locations on the stability of the tunnel, a series of numerical models with the ratio of 1 : 1 were built based on the site geology and construction conditions. As illustrated in Figure 7, the overburden thickness in all models is set as 22 m, among which the fill and clay stratum are 3 m and 19 m thick, respectively. The external diameter of the tunnel is 6.7 m, and the buried depth of the tunnel vault is 13.3 m. The dimension of the entire model in the X and Y directions is 30 m, and the dimension of the model in the Z direction is determined according to the size of the karst cave and the distance between the cave

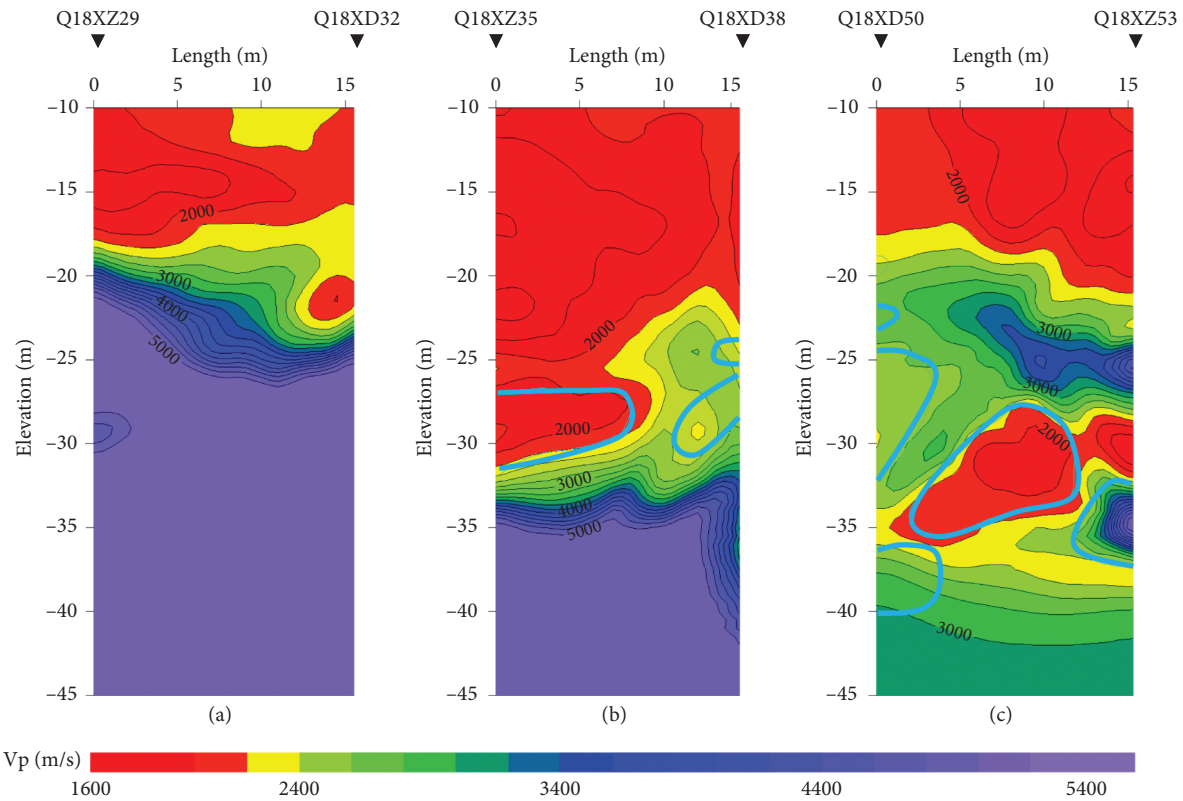

Figure 4: Wave velocity chromatograms of the crosshole seismic CT inversion: (a) without karst profile; (b) karst moderately developed profile; (c) karst strongly developed profile. The blue lines are the interpreted karst caves.

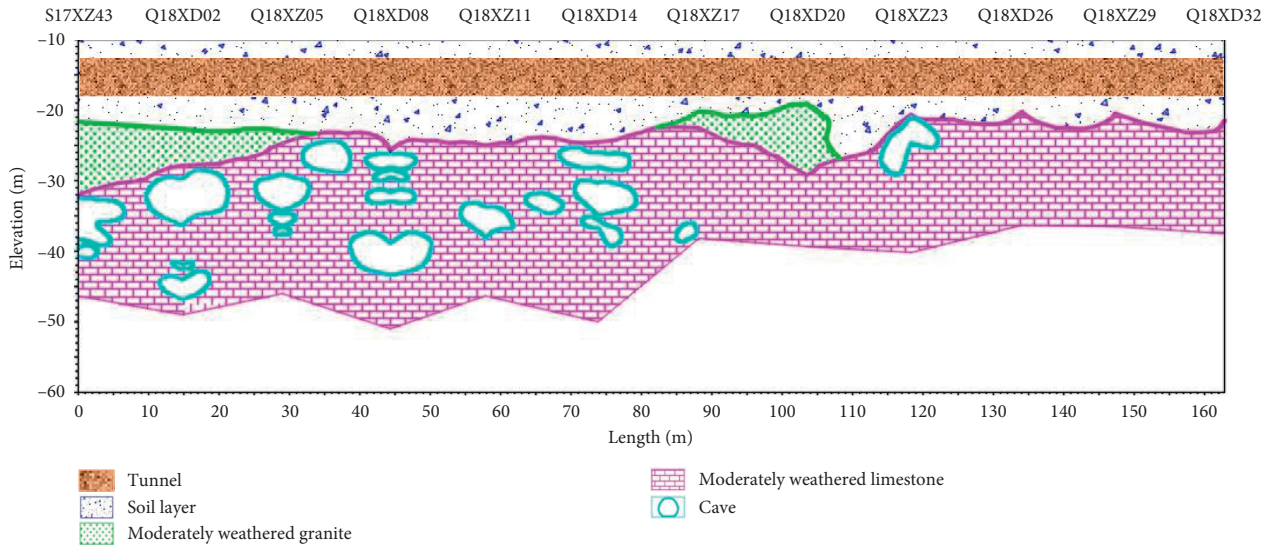

Figure 5: Cross-section view of the karst geology between boreholes S17XZ43-Q18XD32.

and the tunnel. The karst cave, which is simplified in the shape of a sphere, is built beneath the tunnel according to the karst cave survey results in Section 3.2. Considering the symmetry of the model, only one-eighth of the karst cave model is established here to reduce the calculation cost. The radius of the karst cave in the models is varied from 1 m to 5 m, and the distance between them and the tunnel is varied from 3 m to 7 m. In addition, to analyze the effects of different karst cave sizes and the distance between karst cave and tunnel on the tunnel deformation, three monitoring lines were arranged in the axial direction (Y-direction) of the tunnel: tunnel vault monitoring line #1, tunnel haunch

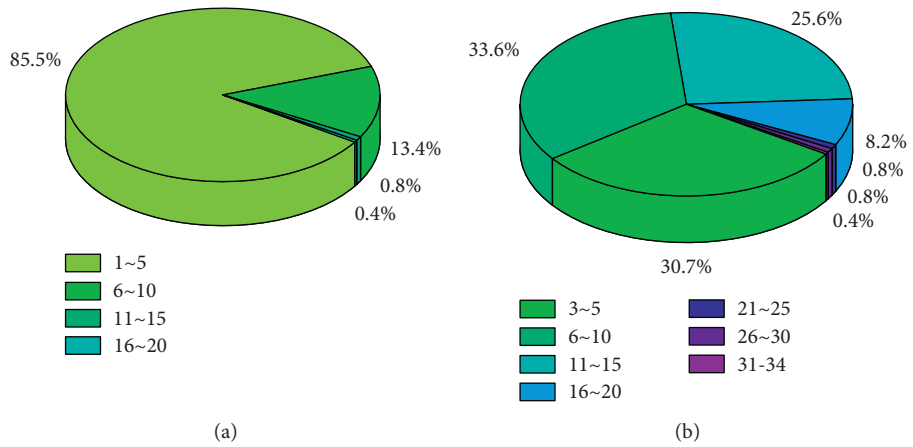

Figure 6: Distribution characteristics of the revealed karst geology in this area. (a) Distribution statistical diagram of the karst cave height. (b) Distribution statistical diagram of the distance between the karst cave and tunnel.

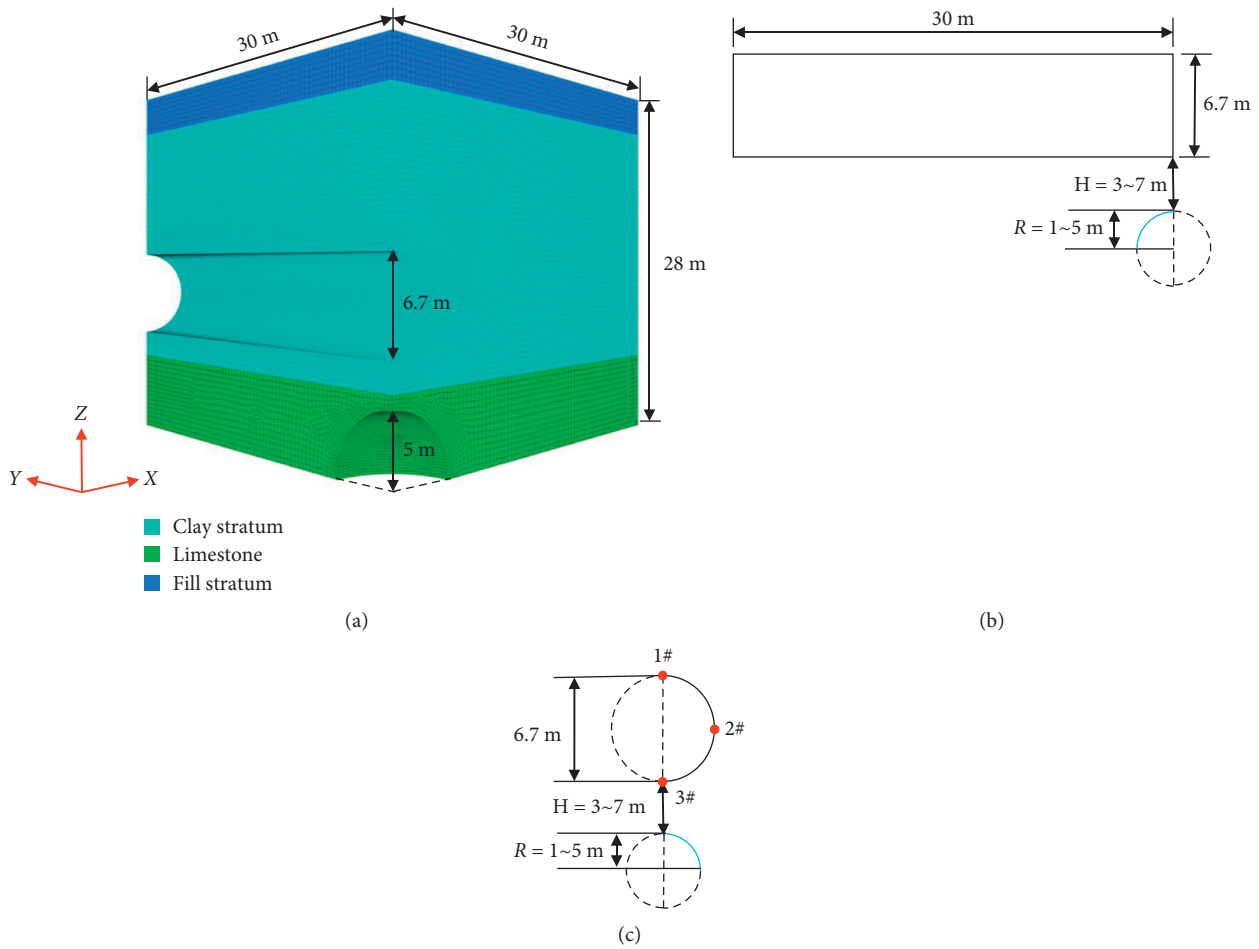

Figure 7: Numerical model and relative positions of the karst cave and tunnel. (a) Numerical model. (b) YZ -section. (c) XZ-section.

monitoring line #2, and tunnel bottom monitoring line #3 (red point in Figure 7(c)).

The Mohr-Coulomb elastic-plastic model was adopted in the numerical calculation. The mechanical parameters of the surrounding soil and rock in tunnels are listed in Table 1, which were obtained from geomechanical testing. The displacement boundary was adopted for the model boundary condition. The lower boundary was fixed with vertical displacement, the front and left boundaries were fixed with horizontal displacement, and the forward and

Table 1: Mechanical parameters of geotechnical materials in the model.

Materials	Gravity (kN/m^3)	Elastic modulus E (MPa)	Poisson's ratio υ	Cohesion c (kPa)	Internal friction angle φ (°)
Fill	20	10	0.3	8	20
Clay	25	15	0.3	14	10
Moderately weathered limestone	25	100	0.3	100	30
Concrete segment	25.4	34500	0.3	/	/

backward boundaries were fixed with axial displacement. Additionally, to simulate the ballast effect of the shield tunneling machine and pedestrian transport materials on the tunnel bottom, a uniform load of 20 kN was applied on the tunnel bottom. The entire simulation is divided into the following steps: (1) establish the model and remove the rock unit at the karst cave; (2) calculate the gravity stress field; (3) remove the soil unit at the tunnel and use liner structural units to simulate the reinforced concrete segments.

4.2. Effect of the Karst Cave Size. To investigate the effect of the sizes of the karst cave on the displacement and stability of the tunnel surrounding rock, the distance between karst cave and tunnel is fixed at 3 m, while the radius of the karst cave is set to 1, 2, 3, 4, and 5 m. Figures 8–10 display the displacements of the tunnel vault (monitoring line #1), waist (monitoring line #2), and bottom (monitoring line #3) at different distances from the karst cave center, which only differ in sizes of the karst cave.

For the tunnel vault displacement, Figure 8 shows that, with the increase in karst cave radius, the change in Z-displacement of tunnel vault increases gradually. When there is no karst cave beneath the tunnel, with the increase in distance from the karst cave center, the Z-displacement of the tunnel vault smoothly changes with subsidence of approximately 18.6 mm. When the radius of the karst cave is 1 or 2 m, the Z-displacement variation of the tunnel vault is almost identical to that without karst cave, and the Z-displacement difference between the two is almost negligible. When the radius of the karst cave increases to 3 m, the Z-displacement of the tunnel vault gradually decreases within the distance of 0–15 m and tends to be stable with subsidence of 18.8 mm within the distance of 15–30 m. Similarly, when the radius of the karst cave increases to 4 m, the Z-displacement of the tunnel vault gradually declines within the distance of 0–18 m and remains at the same level of maximum subsidence of approximately 19.1 mm within the distance of 18–30 m. When the radius of the karst cave increases to 5 m, the Z-displacement of tunnel vault gradually decreases within the distance of 0–19 m and remains stable at maximum subsidence of approximately 19.6 mm within the distance of 19–30 m.

Compared to the case without the karst cave, the subsidence of the tunnel vault decreases near the underlying karst cave and increases far away from the karst cave. A turning point is apparently located at the monitoring section of approximately 11 m from the karst cave center. When the monitoring section is within 0–11 m, the subsidence of the tunnel vault decreases with the increase in the size of the karst cave. When the monitoring section is within 11–30 m, the subsidence of the tunnel vault increases with the increase in the size of the karst cave. Moreover, when the size of the karst cave is small ($R = 1$, 2 m), the change in subsidence of the tunnel vault is basically identical to that without the karst cave, which is almost negligible. However, with the increase in the size of the karst cave ($R = 3$, 4, 5 m), the change in subsidence of the tunnel vault begins to become increasingly obvious, and the corresponding rate of variation is significantly larger than that without the karst cave.

For the tunnel waist displacement, Figure 9 shows that, with the increase in karst cave radius, the change in X-displacement of the tunnel waist gradually increases. When there is no karst cave beneath the tunnel, with the increase in distance from the karst cave center, the X-displacement of the tunnel waist slightly varies at approximately 9 mm. When the radius of the karst cave is 1 or 2 m, the X-displacement variation of tunnel waist is approximately identical to that without the karst cave, and the X-displacement discrepancy between the two is small. Regarding the karst cave with a radius of 3, 4, or 5 m, when the monitoring section is 0–15 m, the corresponding X-displacement of the tunnel waist is less than that without the karst cave, and for a larger cave, the tunnel waist has a smaller corresponding X-displacement. However, when the monitoring section is 15–30 m, the X-displacement tends to the situation where there is no karst cave. In other words, a larger cave size corresponds to a stronger effect on the X-displacement of the tunnel waist closer to the karst cave, which decreases the X-displacement, while the tunnel waist far away from the karst cave is less affected by the karst cave.

For the tunnel bottom displacement, Figure 10 shows that, with the increase in karst cave radius, the change in Z-displacement of the tunnel bottom gradually increases. When there is no karst cave beneath the tunnel, with the increase in distance from the karst cave center, the Z-displacement of the tunnel bottom gently changes with an uplift of approximately 0.44 mm. When the radius of the karst cave is 1 or 2 m, the Z-displacement change of the tunnel bottom is basically identical to that without the karst cave, and the Z-displacement discrepancy between these two cases is practically negligible. Regarding the karst cave with a radius of 3, 4, or 5 m, the Z-displacement of the tunnel bottom gradually increases with the increase in distance from the karst cave center. Moreover, with the increase in the size of the karst cave, the change in Z-displacement of the tunnel bottom

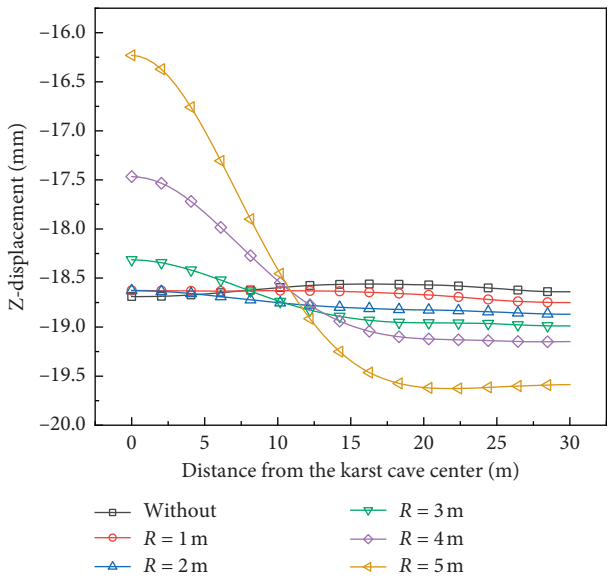

Figure 8: Z-displacement curves of the tunnel vault with varying sizes of the karst cave.

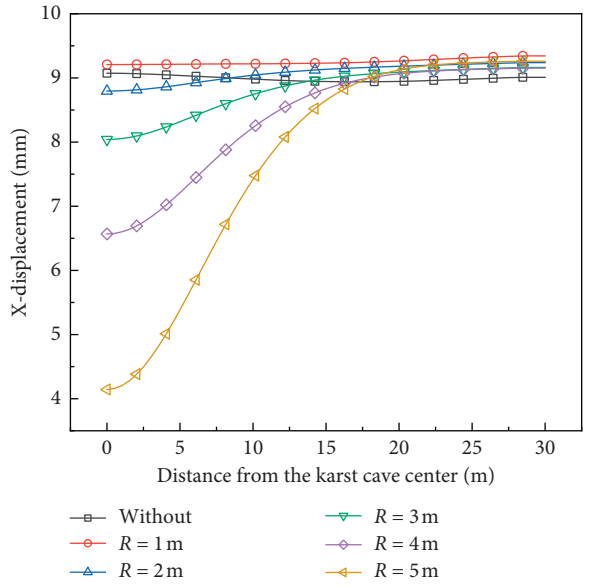

Figure 9: X-displacement curves of the tunnel waist with varying sizes of the karst cave.

begins to become increasingly obvious, and the corresponding change rate is significantly larger than that without the karst cave.

4.3. Effect of the Karst Cave Location. To investigate the effect of the location of the karst cave on the displacement and stability of the tunnel surrounding rock, the radius of the karst cave is fixed at 4 m, while the distance between the karst cave and tunnel is set to 3, 4, 5, 6, and 7 m. Figures 11–13 present the displacement of the tunnel vault (monitoring line #1), waist (monitoring line #2), and bottom (monitoring

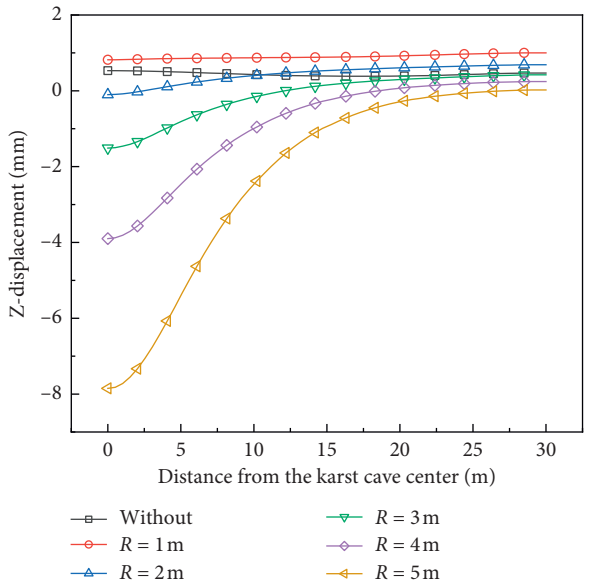

Figure 10: Z-displacement curves of the tunnel bottom with varying sizes of the karst cave.

line #3) at different distances from the karst cave center, which only differ in the location of the karst cave.

For the tunnel vault displacement, Figure 11 shows that, with the increase in distance between the karst cave and tunnel, the change in Z-displacement of tunnel vault gradually decreases. The subsidence displacement of the tunnel vault decreases near the karst cave, and when the tunnel is further from the karst cave, the vault subsidence is greater. When the monitoring section is within 17–30 m, the corresponding vault subsidence tends to be stable. Moreover, with the increase in distance between the karst cave and the tunnel, the subsidence displacement of the tunnel vault increases, the change in subsidence of the tunnel vault begins to become increasingly nonobvious, and the corresponding rate of variation is insignificantly larger than that without the karst cave.

For the tunnel waist displacement, Figure 12 shows that, with the increase in distance between the karst cave and the tunnel, the change in X-displacement of the tunnel waist gradually decreases. The X-displacement of the tunnel waist near the karst cave is small. When the monitoring section is further away from the karst cave, the X-displacement of the tunnel waist gradually increases. When the monitoring section is 15 m from the karst cave center, all X-displacements of the tunnel waist for the five distances between the karst cave and the tunnel gradually tend to be stable at a similar level to that without the karst cave.

For the tunnel bottom displacement, Figure 13 shows that, with the increase in distance between the karst cave and tunnel, the change in Z-displacement of the tunnel bottom gradually decreases. The Z-displacement of the tunnel bottom decreases near the karst cave, and a larger distance between tunnel and karst cave corresponds to a stronger Z-displacement of the tunnel bottom. In addition, there is a

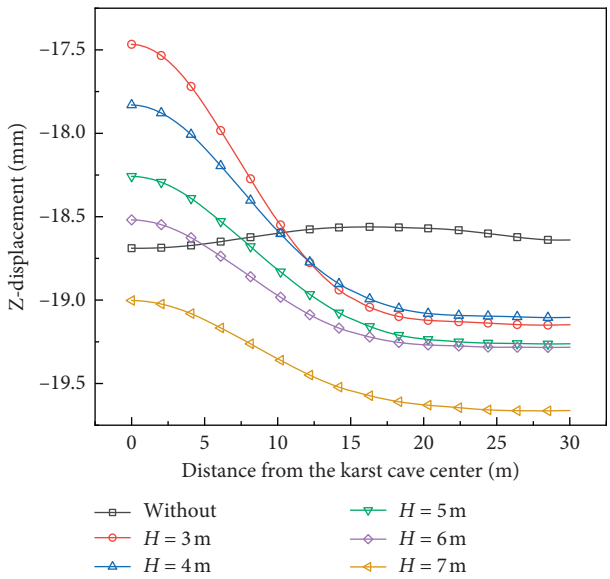

Figure 11: Z-displacement curves of tunnel vault with varying locations of the karst cave.

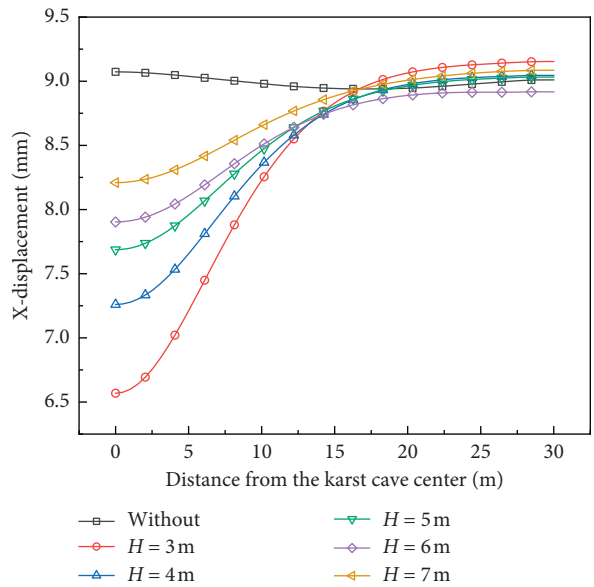

Figure 12: X-displacement curves of the tunnel waist with varying locations of the karst cave.

turning point at the monitoring section of approximately 11 m away from the karst cave center. When the monitoring section is 0–11 m, with the increase in distance between the karst cave and the tunnel, the Z-displacement of the tunnel bottom gradually increases; when the monitoring section is 11–30 m, with the increase in distance between the karst cave and the tunnel, the Z-displacement of the tunnel bottom gradually decreases. In general, with the increase in distance between the karst cave and tunnel, the change amplitude of the Z-displacement gradually decreases, and the corresponding rate of change obviously decreases.

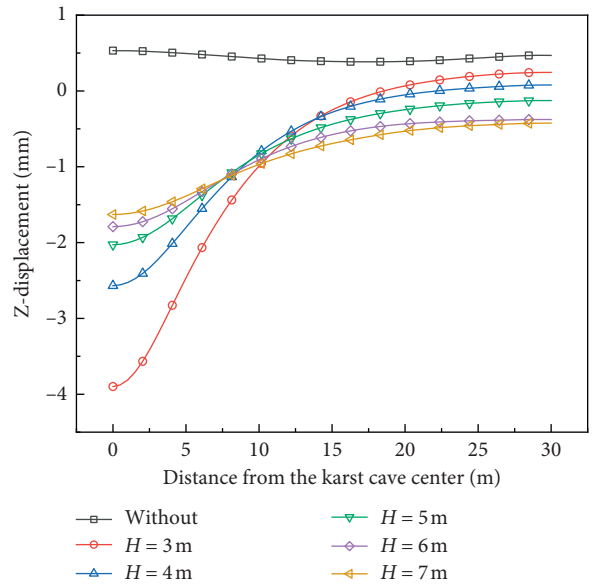

Figure 13: Z-displacement curves of the tunnel bottom with varying locations of the karst cave.

4.4. Risk Assessment of Tunnel Collapse. According to the simulation results described in Sections 4.2 and 4.3, the deformation discrepancy (at the vault, waist, or bottom) of different monitoring sections of the tunnel is increasingly obvious with the increase in the size of the karst cave and decrease in distance between the tunnel and the karst cave. To characterize the influence extent of the karst cave on the deformation discrepancy of different monitoring sections of the tunnel, a representative index called the disturbance degree is established, which is defined by the ratio of the maximum displacement discrepancy of different monitoring sections of the tunnel to the radius of the tunnel. A detailed comparison of the disturbance degree with varying sizes and locations of the karst cave is presented in Figure 14. The disturbance degree exponentially increased with the increase in radius of the cave and with the decrease in distance between the tunnel and karst cave. The influence of the size of the karst cave and the distance between the karst cave and tunnel on the disturbance degree of the tunnel bottom is more significant than that of the vault and tunnel waist. Thus, the disturbance degree of the tunnel bottom can be used to represent the influence degree of the karst cave on the deformation of the tunnel. A greater disturbance degree of the tunnel bottom corresponds to a stronger effect of the karst cave on the tunnel deformation.

The development law of plastic zone under different sizes and locations of the karst cave is presented in Figure 15. The plastic zone of the karst cave appears mainly near the arch toe and develops along the tangent direction of the arch with the increase in radius of the karst cave (Figure 15(a)). Thus, the karst cave is mainly damaged by the shear of the arch toe. In this case, the overburden soil from the roof plate to the bottom of the tunnel will eventually collapse, forming a cone-dish collapse pit at the bottom of the tunnel. When the

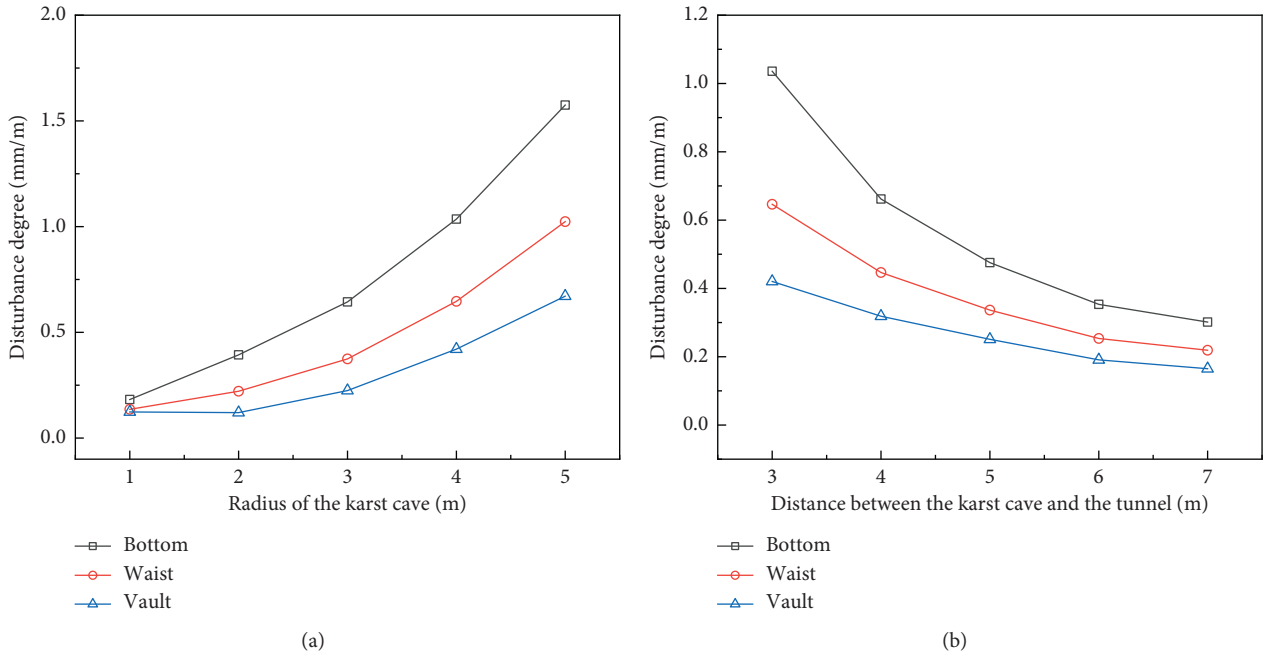

Figure 14: Change law of the disturbance degree with (a) varying sizes and (b) locations of the karst cave.

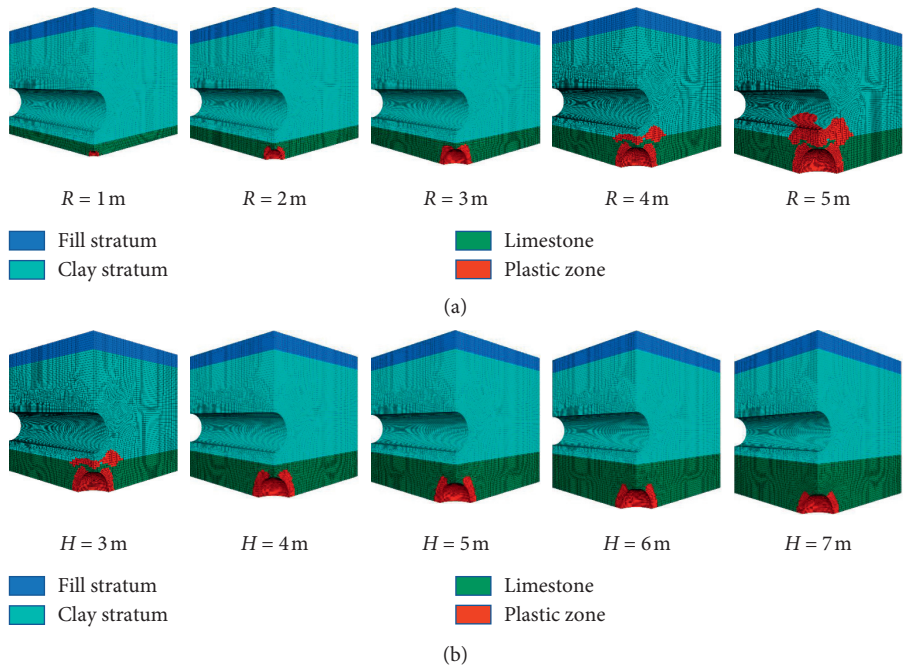

Figure 15: Development law of the plastic zone under different sizes (a) and locations (b) of the karst cave.

size of the karst cave is small ($R = 1$ or 2 m), the plastic zone only appears in the local area of the limestone layer; when the size of the cave further increases ($R = 3$, 4, or 5 m), the plastic zone penetrates the limestone layer where the cave is located and extends to the clay stratum where the tunnel is located, causing collapse accidents during the tunnel construction. Additionally, when the size of the karst cave is fixed at a radius of 4 m, the plastic zone of the karst cave gradually shrinks to the arch toe with the increase in distance between the karst cave and tunnel (Figure 15(b)). Thus, a greater distance between the karst cave and tunnel has a weaker effect on the stability of the tunnel surrounding rock.

By comparing Figures 14 and 15, it can be found that the development law of the disturbance degree is completely consistent with that of the plastic zone. When the size of the karst cave is relatively small ($R < 4$ m in Figure 15(a)) and the distance between the karst cave and tunnel is considerably large ($H > 3$ m in Figure 15(b)), the disturbance degree of the

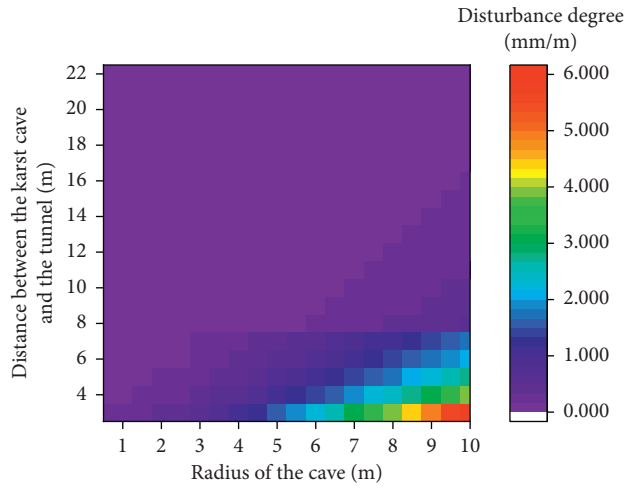

Figure 16: Heat map of the disturbance degree of the karst cave to the tunnel under all karst distribution conditions.

karst cave to the tunnel deformation is less than 1 mm/m. At this time, the plastic zone is only distributed near the arch toe of the karst cave in the limestone layer and has not penetrated the upper clay layer, indicating that the surrounding rock of the tunnel is stable. However, when the size of the karst cave increases ($R = 4$ or 5 m in Figure 15(a)) and the distance between the karst cave and tunnel decreases ($H = 3$ m in Figure 15(b)), the disturbance degree of the karst cave to the tunnel deformation has exceeded 1 mm/m, and the plastic zone has penetrated the upper clay layer. Thus, the disturbance degree can represent the stability of the surrounding rock of the tunnel, and the disturbance degree of 1 mm/m can be taken as the safety threshold for the stability of the tunnel. When the disturbance degree is greater than 1 mm/m, the surrounding rock of the tunnel can be considered unstable, and tunnel collapse may occur. In this case, the karst cave must be filled by single slurry or binary slurry before tunnel construction to eliminate the risk of tunnel collapse [22].

According to the detection results of the characteristics of karst development in Section 3, the disturbance degree of the karst cave to the tunnel under all karst distribution conditions is calculated and plotted in Figure 16. Different color blocks are used to distinguish the disturbance degree of the karst cave to the tunnel in Figure 16. A closer color to red corresponds to a larger disturbance degree; a closer color to purple corresponds to a smaller disturbance degree. Figure 16 shows that the buried depth of the karst cave greatly affects the disturbance degree. For a deeply buried karst cave (the distance between the cave and the tunnel is greater than 7 m), the disturbance degree to the tunnel is less than 1 mm/m even when the radius of the cave is 10 m, implying that no treatment is required for karst caves buried deeper than 7 m. For a relatively shallow buried karst cave, that is, the distance between the cave and tunnel is less than 7 m, there is a critical value for the cave size. When the size is larger than the critical value, the disturbance degree to the tunnel will exceed the safety threshold. For example, when the distance between the karst cave and the tunnel is 7 m and 6 m, the critical dimensions are 7 m and 6.5 m, respectively.

5. Conclusions

This paper presents a synthetic method to evaluate the collapse risk where there is a karst cave beneath a metro tunnel. The methodology consists of two components: an accurate karst exploration to precisely detect the distribution characteristics of the karst caves based on geophysical technique and a quantitative assessment to evaluate the effect of the karst cave on tunnel collapse based on numerical simulation.

In the detection of the location and scale of karst, the crosshole seismic CT was applied to record 483 groups of seismic wave CT images, and 524 karst cave anomalies were found in total. The height of karst caves in the study area is 1–20 m and mainly concentrated at approximately 5 m. The vertical distance between the karst cave and tunnel is mainly within 15 m, among which 6–10 m accounts for the largest portion, which is 33.6%.

To investigate the effect of different sizes and locations of karst caves on the displacement and stability of the surrounding rock in tunnels, a series of numerical models were built and calculated using FLAC3D according to the results obtained from the geophysical detection. The simulation results indicate that, compared to the absence of karst caves, the existence of karst caves makes the deformation of the monitoring sections at different positions of the tunnels different, and with the increase in the size of the karst cave and decrease in distance between the karst cave and the tunnel, the deformation discrepancy becomes increasingly significant.

The definition of the disturbance degree of the karst cave to the tunnel deformation was provided. The disturbance degree under different sizes and locations of the karst cave was calculated and compared with the distribution characteristics of the plastic zone. It can be found that the development law of the disturbance degree is completely consistent with that of the plastic zone. Then, the disturbance degree was taken as a quantitative evaluation index of tunnel stability, and the karst caves with a disturbance degree greater than 1 mm/m were evaluated as those that must be disposed of.

The disturbance degree evaluation results for all karst distribution conditions indicate that the buried depth of the karst cave greatly affects the disturbance degree. No treatment is required for the deeply buried karst cave whose distance from the tunnel exceeds 7 m. When the distance between the cave and the tunnel is less than 7 m, there is a critical value for the size of the cave. The karst caves that are larger than that critical value must be filled by single slurry or binary slurry before tunnel construction to eliminate the risk of tunnel collapse.

Data Availability

The data used to support the findings of this study are available from the corresponding author upon request.

Conflicts of Interest

The authors declare that they have no conflicts of interest in this work.

Acknowledgments

The authors would like to acknowledge the financial support for this study provided by the Natural Science Foundation of Zhejiang Province (LQ20E080006), the Shaoxing Public Interest Research Projects (2017B70002), and the Research Projects of Shaoxing University in 2018 (2018LG1004).

References

[1] Y. Wang, H. Jing, L. Yu, H. Su, and N. Luo, "Set pair analysis for risk assessment of water inrush in karst tunnels," *Bulletin of Engineering Geology and the Environment*, vol. 76, no. 3, pp. 1199–1207, 2017.

[2] S. C. Li, Z. Q. Zhou, Z. H. Ye, L. P. Li, Q. Q. Zhang, and Z. H. Xu, "Comprehensive geophysical prediction and treatment measures of karst caves in deep buried tunnel," *Journal of Applied Geophysics*, vol. 116, pp. 247–257, 2015.

[3] S. C. Li, J. Wu, Z. H. Xu, L. Zhou, and B. Zhang, "A possible prediction method to determine the top concealed karst cave based on displacement monitoring during tunnel construction," *Bulletin of Engineering Geology and the Environment*, vol. 78, no. 1, pp. 341–355, 2019.

[4] L. Zini, C. Chiara, and C. Franco, "The challenge of tunneling through Mediterranean karst aquifers: the case study of Trieste (Italy)," *Environmental Earth Sciences*, vol. 74, no. 1, pp. 281–295, 2015.

[5] M. E. Collins, M. Cum, and P. Hanninen, "Using ground-penetrating radar to investigate a subsurface karst landscape in north-central Florida," *Geoderma*, vol. 61, no. 1-2, pp. 1–15, 1994.

[6] A. T. Chamberlain, W. Sellers, C. Proctor, and R. Coard, "Cave detection in limestone using ground penetrating radar," *Journal of Archaeological Science*, vol. 27, no. 10, pp. 957–964, 2000.

[7] W. Al-Fares, M. Bakalowicz, R. Guérin, and M. Dukhan, "Analysis of the karst aquifer structure of the Lamalou area (Hérault, France) with ground penetrating radar," *Journal of Applied Geophysics*, vol. 51, no. 2-4, pp. 97–106, 2002.

[8] B. Liu, Z. Liu, S. Li et al., "Comprehensive surface geophysical investigation of karst caves ahead of the tunnel face: a case study in the Xiaoheyan section of the water supply project from Songhua River, Jilin, China," *Journal of Applied Geophysics*, vol. 144, pp. 37–49, 2017.

[9] J. Cheng, F. Li, S. Peng, X. Sun, J. Zheng, and J. Jia, "Joint inversion of TEM and DC in roadway advanced detection based on particle swarm optimization," *Journal of Applied Geophysics*, vol. 123, pp. 30–35, 2015.

[10] P. Asadollahi and R. Foroozan, "Comparison of the evaluated rock mass properties from the TSP system and the RMR classification (Semnan tunnel, Iran)," *Tunnelling and Underground Space Technology*, vol. 21, no. 3-4, p. 236, 2006.

[11] A. Alimoradi, A. Moradzadeh, R. Naderi, M. Z. Salehi, and A. Etemadi, "Prediction of geological hazardous zones in front of a tunnel face using TSP-203 and artificial neural networks," *Tunnelling and Underground Space Technology*, vol. 23, no. 6, pp. 711–717, 2008.

[12] G. Chen, Z.-Z. Wu, F.-J. Wang, and Y.-L. Ma, "Study on the application of a comprehensive technique for geological prediction in tunneling," *Environmental Earth Sciences*, vol. 62, no. 8, pp. 1667–1671, 2011.

[13] G. Huang, B. Zhou, H. Li, H. Zhang, and Z. Li, "2D seismic reflection tomography in strongly anisotropic media," *Journal of Geophysics and Engineering*, vol. 11, no. 6, Article ID 065012, 2014.

[14] Y. Rao, Y. Wang, S. Chen, and J. Wang, "Crosshole seismic tomography with cross-firing geometry," *Geophysics*, vol. 81, no. 4, pp. R139–R146, 2016.

[15] Y. Albouy, P. Andrieux, G. Rakotondrasoa et al., "Mapping coastal aquifers by joint inversion of DC and TEM soundings-three case histories," *Groundwater*, vol. 39, no. 1, pp. 87–97, 2005.

[16] D. Gomez-Ortiz and T. Martin-Crespo, "Assessing the risk of subsidence of a sinkhole collapse using ground penetrating radar and electrical resistivity tomography," *Engineering Geology*, vol. 149-150, pp. 1–12, 2012.

[17] S. D. Carriere, K. Chalikakis, G. Senechal, C. Danquigny, and C. Emblanch, "Combining electrical resistivity tomography and ground penetrating radar to study geological structuring of karst unsaturated zone," *Journal of Applied Geophysics*, vol. 94, pp. 31–41, 2013.

[18] E. Cardarelli, M. Cercato, A. Cerreto et al., "Electrical resistivity and seismic refraction tomography to detect buried cavities," *Geophysical Prospecting*, vol. 58, no. 4, pp. 685–695, 2010.

[19] C. Duan, C. Yan, B. Xu, and Y. Zhou, "Crosshole seismic CT data field experiments and interpretation for karst caves in deep foundations," *Engineering Geology*, vol. 228, pp. 180–196, 2017.

[20] J. Tronicke, H. Paasche, and U. Böniger, "Crosshole travel time tomography using particle swarm optimization: a near-surface field example," *Geophysics*, vol. 77, no. 1, pp. R19–R32, 2012.

[21] Y. Zhao, Q. Peng, W. Wan, W. Wang, and B. Chen, "Fluid-solid coupling analysis of rock pillar stability for concealed karst cave ahead of a roadway based on catastrophic theory," *International Journal of Mining Science and Technology*, vol. 24, no. 6, pp. 737–745, 2014.

[22] Q.-L. Cui, H.-N. Wu, S.-L. Shen, Y.-S. Xu, and G.-L. Ye, "Chinese karst geology and measures to prevent geohazards during shield tunnelling in karst region with caves," *Natural Hazards*, vol. 77, no. 1, pp. 129–152, 2015.

[23] Z. Song, "Research on the influence of concealed karst caves upon the stability of tunnels and its support structure," *Chinese Journal of Rock Mechanics and Engineering*, vol. 25, no. 6, p. 1296, 2016.

[24] Y. Lai, *Study on Safe Distance between Concealed Karst Cave and Tunnel and its Intelligent Prediction Model*, Beijing Jiaotong University, Beijing, China, 2012.

[25] F. Huang, L. Zhao, T. Ling, and X. Yang, "Rock mass collapse mechanism of concealed karst cave beneath deep tunnel," *International Journal of Rock Mechanics and Mining Sciences*, vol. 91, pp. 133–138, 2017.